

RoadBench: Benchmarking MLLMs on Fine-Grained Spatial Understanding and Reasoning under Urban Road Scenarios

Jun Zhang¹, Jie Feng^{1†}, Long Chen², Junhui Wang², Zhicheng Liu², Depeng Jin¹, Yong Li^{1†}

¹Department of Electronic Engineering, BNRist, Tsinghua University, Beijing, China

²Amap, Alibaba Group, Beijing, China

{fengjie, liyong07}@tsinghua.edu.cn

Abstract

Multimodal large language models (MLLMs) have demonstrated powerful capabilities in general spatial understanding and reasoning. However, their fine-grained spatial understanding and reasoning capabilities in complex urban scenarios have not received significant attention in the fields of both research and industry. To fill this gap, we focus primarily on road markings as a typical example of fine-grained spatial elements under urban scenarios, given the essential role of the integrated road traffic network they form within cities. Around road markings and urban traffic systems, we propose **RoadBench**, a systematic benchmark that comprehensively evaluates MLLMs' fine-grained spatial understanding and reasoning capabilities using BEV and FPV image inputs. This benchmark comprises six tasks consisting of 9,121 strictly manually verified test cases. These tasks form a systematic evaluation framework that bridges understanding at local spatial scopes to global reasoning. They not only test MLLMs' capabilities in recognition, joint understanding, and reasoning but also assess their ability to integrate image information with domain knowledge. After evaluating 14 mainstream MLLMs, we confirm that **RoadBench** is a challenging benchmark for MLLMs while revealing significant shortcomings in existing MLLMs' fine-grained spatial understanding and reasoning capabilities within urban scenarios. In certain tasks, their performance even falls short of simple rule-based or random selection baselines. These findings, along with **RoadBench** itself, will contribute to the comprehensive advancement of spatial understanding capabilities for MLLMs.

1. Introduction

Multimodal large language models (MLLMs) have become a crucial tool for recognizing and understanding the real world due to their powerful combined visual-language com-

[†]Corresponding author

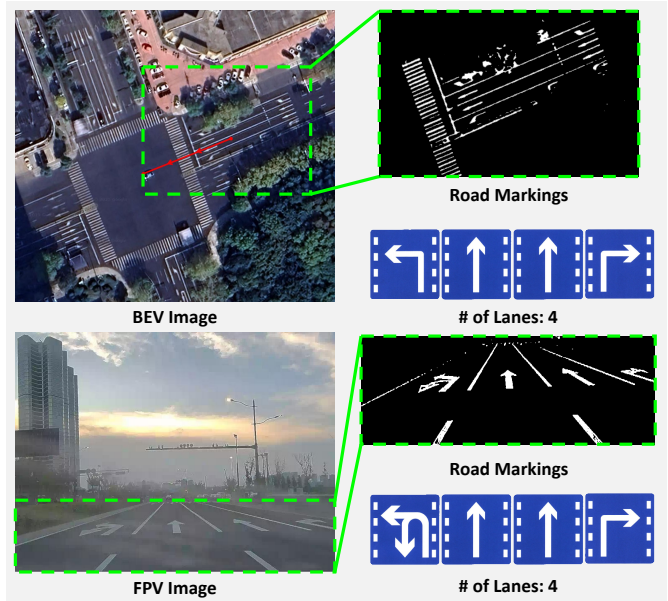


Figure 1. Examples of road markings in BEV and FPV images with their meanings.

prehension and reasoning capabilities [1, 3, 31, 42]. They are progressively replacing specialized models in fields such as satellite image recognition [15, 45, 46], autonomous driving [10, 33, 47], embodied intelligence [12, 22], etc. Spatial understanding and reasoning in urban environments, as one of the key real-world application scenarios for MLLMs, have also garnered significant attention recently [14, 15, 30]. Various research efforts have released benchmarks [16, 39, 50] for spatial understanding and reasoning tasks in urban environments, evaluating MLLM performance from multiple perspectives. These benchmarks provide the foundational data and evaluation criteria necessary to advance MLLM research for real-world applications.

However, we observe that existing benchmarks on urban scenarios mainly focus on whole-image-level understanding or isolated object recognition of specific types, such as

GeoQA, landmark recognition, and vehicle detection. There appears to be a lack of attention to understanding and reasoning about fine-grained spatial elements within urban scenarios. Recently, cutting-edge research has been exploring how to enhance MLLM’s fine-grained understanding and reasoning capabilities in scenarios such as mathematical problems [44] and remote sensing images [26]. Nevertheless, studies on MLLM’s such capabilities have yet to be applied to urban scenarios, particularly lacking evaluation benchmarks tailored to real-world urban settings.

Under urban scenarios, a representative example of such fine-grained spatial structural elements is the markings painted on city road surfaces shown in Figure 1. These narrow and long lines and arrows, drawn based on specialized traffic knowledge, collectively form an integrated system that effectively divides and organizes urban space, thereby regulating the movement of pedestrians and vehicles. The tasks of understanding and reasoning about road markings pose significant challenges to MLLM’s capabilities:

- The ability to recognize fine-grained structures at a global scale, as road markings are typically thin and extend across the entire image.
- The joint understanding and reasoning of multiple fine-grained structures, as road markings require overall consideration for accurate semantic recognition.
- The integration of image information and domain knowledge to generate reasonable responses.

We believe that developing MLLM’s fine-grained understanding and reasoning capabilities under urban scenarios will not only advance its applications in transportation fields, such as high-definition map auto-generation and end-to-end autonomous driving. It will also enhance MLLM’s general visual-spatial reasoning abilities, particularly regarding various artificially designed symbol and marking systems in other fields.

Therefore, we propose **RoadBench**, a systematic benchmark primarily designed to evaluate MLLM’s understanding and reasoning capabilities regarding fine-grained spatial structural elements under urban scenarios. RoadBench provides a rich collection of annotated Bird’s-Eye View (BEV) and First-Person View (FPV) images, comprising a total of 9,121 test cases across 6 tasks. These tasks include not only lane counting and lane designation recognition, which are directly based on understanding and reasoning about road markings, but also extend to road network correction and road type classification tasks that rely on joint reasoning involving both road markings and other information within the image. The test cases comprising RoadBench originate from manually selected images across multiple major cities. All labels and ground truth data have been labeled and checked by humans to ensure accuracy, with all potentially privacy-sensitive information completely masked and anonymized. These test cases encompass diverse factors that may impact

MLLM understanding, including road and intersection patterns, lighting conditions, seasons, and image resolution. This comprehensively supports the systematic evaluation of MLLM’s fine-grained spatial understanding and reasoning capabilities. Based on RoadBench, we conducted a systematic evaluation of 14 mainstream closed-source and open-source MLLMs. Benchmark results indicate that MLLMs failed to achieve satisfactory outcomes across various tasks, even underperforming against baselines based on random choice or simple rules in certain tasks. This highlights both the current limitations of MLLMs in achieving fine-grained spatial understanding and reasoning capabilities within urban environments, and underscores RoadBench as a highly challenging benchmark for MLLMs to evaluate such capabilities.

Overall, the main contributions of this paper include the following points:

- We propose a systematic benchmark named **RoadBench**, designing six tasks under both BEV and FPV image inputs to comprehensively evaluate MLLMs’ understanding and reasoning capabilities regarding fine-grained spatial elements under urban scenarios from local to global scopes.
- We collected, processed, and annotated 9,121 test cases as datasets for the six tasks in RoadBench using data sources such as satellite imagery, online map service providers, and crowd-sourced in-vehicle camera photo databases. All test cases underwent rigorous manual verification and annotation to ensure the accuracy of their labels.
- We conducted a systematic evaluation of 14 mainstream MLLMs using RoadBench. The results demonstrate that RoadBench is a highly challenging benchmark for MLLMs, while also revealing the limitations of existing MLLMs in fine-grained spatial understanding and reasoning capabilities within urban scenarios.

2. Related Work

2.1. MLLM for Spatial Intelligence

Inspired by the powerful comprehension and complex reasoning capabilities emerging from large language models [4, 34], researchers have achieved alignment and fusion between text and image modalities through techniques such as CLIP [28] and BLIP [21] to construct multimodal large language models (MLLMs) [1, 3, 31, 42]. These MLLMs can simultaneously process textual and visual inputs to perform comprehension and reasoning tasks, enabling them to accomplish a wide range of complex operations [10, 38]. Additionally, some recent researchers have focused on enhancing MLLM’s fine-grained spatial understanding and reasoning capabilities in scenarios such as mathematical problems [24, 37, 44], daily images [2, 6, 8, 18], abstract vi-

sual puzzles [29, 35], and remote sensing images [19, 26, 40]. Leveraging the capabilities of MLLM foundation models, some researchers have successfully developed MLLMs specifically tailored for urban scenarios, such as UrbanLLaVA [14, 15], Embodied-R [48], VLDrive [43] and Spatial-LLM [7]. However, research on the fine-grained understanding and reasoning capabilities of MLLM in urban scenarios remains relatively rare at present. The lack of benchmarks may be one of the primary factors constraining such work.

2.2. Spatial Benchmarks for MLLM

In recent years, researchers have released extensive benchmarks for MLLMs. For example, MME [17], Seedbench [20], and MMBench [23] introduce various perception, cognition, and reasoning tasks to comprehensively evaluate the performance of MLLMs. Some recent researchers have also developed benchmarks using abstract visual puzzles to evaluate the spatial reasoning capabilities of MLLMs, for example, SPACE [29], SpatialEval [35], and Spatial457 [36]. VSI-Bench [41] and MM-Spatial [11] evaluate the spatial understanding and reasoning abilities of MLLMs with indoor environment. In real-world urban scenarios, CityBench [16] primarily evaluates MLLM’s ability to perceive and understand images about cities, as well as its planning and decision-making capabilities. UrBench [50] focuses on evaluating MLLMs in cross-view urban scenarios. CityEQA [49] investigates the urban scenarios from the aerial vehicle in a realistic 3D urban simulator. DriveBench [39] and NuPlanQA [27] focus on evaluating the reliability of MLLM and multi-view understanding abilities in autonomous driving applications. MapDR [5] is a benchmark dataset designed to evaluate the ability of MLLMs to understand and interpret driving rules through traffic signs. Overall, as shown in Table 1, there is currently no benchmark attentive to the recognition, understanding, or reasoning of fine-grained spatial elements with strong interdependency like road markings under urban scenarios, which limits the evaluation of MLLM capabilities in real world scenarios.

3. RoadBench

3.1. Benchmark Overview

RoadBench is designed as a benchmark to evaluate the fine-grained spatial understanding and reasoning capabilities of MLLM models in urban scenarios. As shown in Figure 2, RoadBench contains two types of urban scene images: bird’s eye view images derived from satellite imagery and first-person view images captured by in-vehicle cameras. Based on these two categories of images, we design six benchmark tasks centered around road markings, which are common fine-grained spatial elements in urban scenarios. These tasks are organized in order of the spatial scope from local

to global that MLLM requires for task completion, collectively forming a hierarchical and systematic benchmark that spans from fine-grained local perception and understanding to global contextual reasoning. The number of test cases included in each task is also shown in Figure 2. The entire benchmark comprises a total of 9,121 test cases. These rigorously hand-curated and processed test cases cover diverse scenarios involving different road and intersection patterns, lighting conditions, seasons, and image resolutions, providing comprehensive coverage of the diversity in urban environments.

3.2. Benchmark Tasks

The six benchmark tasks in RoadBench include lane counting and lane designation recognition using BEV images and FPV images, respectively, as well as road network correction using BEV images and road type classification using FPV images. Each task’s setup and evaluation method will be introduced below. The specific MLLM prompts used, typical MLLM input images, and MLLM responses can be found in Appendix 6.

BEV Lane Counting. The lane counting task based on BEV images requires the MLLM to determine the number of lanes contained within the road indicated by the reference line, using the input satellite image and the additional directed reference line. As shown in the example in Appendix 6.1, reference lines are drawn as polylines with prominent red arrows on satellite imagery to serve as visual prompts. The MLLM’s output is required to be a text describing the reasoning process along with the number of lanes. This task aims to conduct a preliminary evaluation of MLLM’s ability to follow both visual and textual prompts simultaneously while analyzing and understanding the narrow road markings surrounding reference lines in satellite imagery. The coordinates of reference lines and actual lane counts in test cases originate from the databases of a tier-1 online map service provider, which also supplies this data for online service delivery. In terms of evaluation metrics, we employed multi-class classification metrics (Precision, Recall, F1-score) on one hand, while also utilizing RMSE to assess the deviation between MLLM outputs and ground truth.

BEV Lane Designation Recognition. The lane designation recognition task based on BEV images shares the same MLLM input setup as the BEV lane counting task, including satellite images and reference lines. In difference, this task further requires MLLM to infer the direction type of each lane by identifying and understanding road surface arrows, among other methods, when the correct number of lanes is known. Lane direction types include U-turn, left turn, straight ahead, right turn, and their combinations. This task not only challenges the MLLM’s ability to jointly understand a complete set of road markings, but also tests its domain

Table 1. Comparison of spatial benchmarks for MLLM under real-world urban scenarios.

Benchmark	Minimum Spatial Granularity	Element Inter-dependency	Viewpoint
CityBench [16]	★ (buildings)	★ (isolated elements)	BEV + FPV
UrBench [50]	★★ (traffic signs)	★★ (cross-view matching)	BEV + FPV
CityEQA [49]	★★ (cars & buildings)	★ (isolated elements)	3D Scene (synthetic)
DriveBench [39]	★★ (cars)	★ (isolated elements)	FPV
NuPlanQA [27]	★★ (cars & traffic signs)	★★ (trajectory reasoning)	BEV + FPV
MapDR [5]	★★ (lanes & traffic signs)	★★ (rule-lane matching)	FPV
RoadBench	★★★ (road markings)	★★★ (topological + regulatory logic)	BEV + FPV

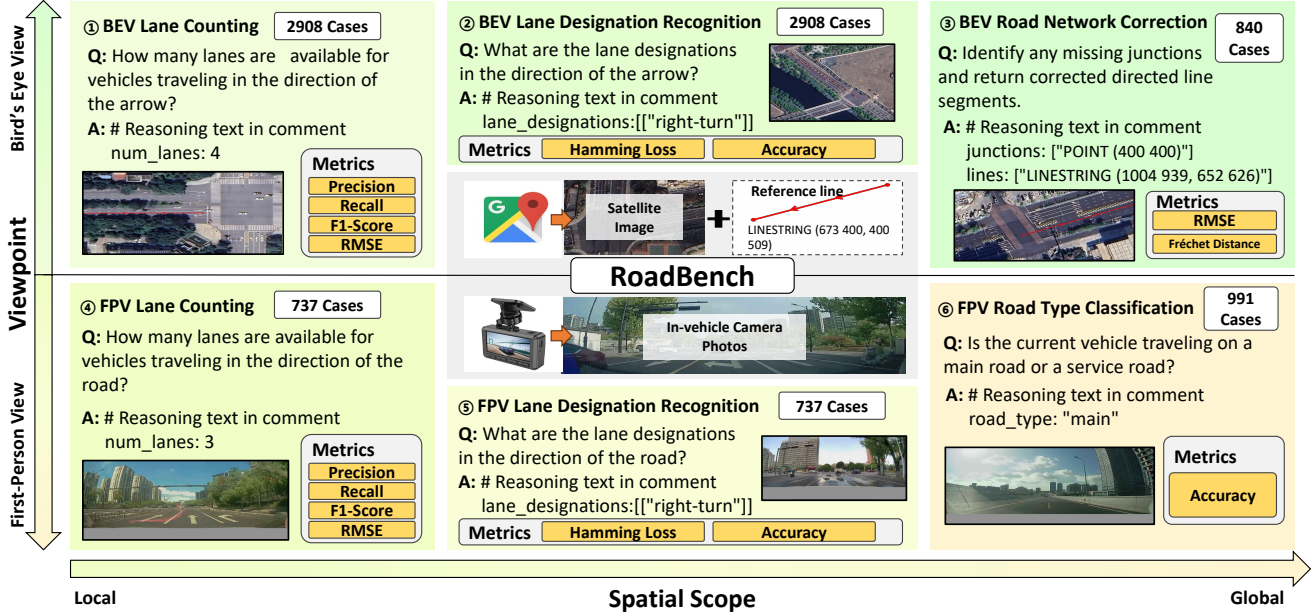


Figure 2. The overview of RoadBench.

expertise in lane designation. Ground truth data also comes from the online service database. Given the combinatorial nature of lane directions, we treat the classification of each lane as an independent multi-label classification problem. We employ the Hamming Loss as the primary metric and utilize accuracy as a more stringent metric to evaluate whether MLLMs fully comprehend the lane directions.

BEV Road Network Correction. The road network correction task based on BEV images is both highly challenging and of significant practical value. This task begins by feeding an inaccurate reference line into MLLMs. These reference lines often contain errors such as missing actual junctions, which can lead to map services providing incorrect directions to users. MLLMs are tasked with understanding the concepts of junctions and road segments, then inferring the correct junction locations and road segments based on the diverse information contained within the images to achieve road network correction. In this task, MLLMs have to recognize not only the image content within the reference line area but also understand broader contextual information such as vehicle

orientation and building layout to determine whether any junctions are missing. The reference lines for this task are sourced from OpenStreetMap¹, and the actual junction and road segment data also originate from the online map service database. The evaluation of results is divided into two parts: the accuracy of junction points and the accuracy of road segment polylines. Since the number of points and polylines returned by MLLMs may not match the ground truth, both evaluations will first match the ground truth with the MLLM output based on the nearest-neighbor principle. Points or polylines that fail to match will be considered as mapped to infinity. Point matching employs Euclidean distance, and RMSE with a distance upper bound threshold is used as the evaluation metric. For polylines, given the critical role of direction in road network correction, we employ the Fréchet Distance [13], which evaluates directed polyline similarity, as both a distance criterion and a performance metric. This metric also incorporates a distance upper bound. Additionally, since image sizes vary, all coordinates are normalized to

¹<https://www.openstreetmap.org/>

the range $[0, 1]$ based on the image length and width before entering the indicator calculation.

FPV Lane Counting. Similar to the BEV lane counting task, the lane counting task based on FPV images also requires the MLLM to determine the number of lanes from images, sharing identical evaluation metrics and ground truth data sources. The difference lies in replacing the image perspective with a first-person view captured by an in-vehicle camera. Simultaneously, the reference lines indicating the target road on the BEV image are removed, requiring MLLMs to understand the spatial relationship between the camera and the surrounding roads to make determinations.

FPV Lane Designation Recognition. The lane designation recognition task based on FPV images shares identical metrics and ground truth data sources with BEV lane designation recognition task. Compared to the BEV perspective, which relies entirely on road markings to identify lane direction, MLLMs in the FPV perspective can determine lane direction both through road markings and by confirming overhead signs. However, FPV images also introduce new challenges for MLLMs. Scenes captured by FPV cameras may include low-light conditions at night or situations where congested traffic obscures road markings. The real-world scenarios reflected in this data will test MLLMs’ ability to synthesize information from multiple sources and produce accurate reasoning.

FPV Road Type Classification. The road type classification task based on FPV images requires MLLMs to determine whether the current vehicle is traveling on the main road or the service road based on the image content. Unlike other tasks, this task demands that MLLMs go beyond understanding and reasoning about a single category of urban spatial elements, such as road markings or even road networks. Instead, it requires MLLMs to grasp the semantic information implied by the surrounding environment as a whole and to make inferences based on common sense. For example, MLLMs can determine whether a road is a service road based on pedestrians or street-side shops in an image, or identify a main road based on enclosed fences and median strips. Since the dataset construction ensures an equal distribution of test cases between the main and service roads, this constitutes a balanced binary classification task. Thus, the evaluation metric solely employs accuracy.

In summary, the aforementioned six benchmark tasks systematically evaluate MLLM’s ability to understand and reason about fine-grained spatial elements in urban environments across spatial scales from local to global based on images captured from diverse perspectives and scenes.

3.3. Benchmark Curation

The curation process for RoadBench can be divided into three stages as shown in Figure 3: data preparation, data processing, and quality control. To fully ensure data quality,

most steps rely primarily on human expert annotation and rule-driven programmatic automatic matching.

Data Preparation. For tasks related to BEV images, the primary step in data preparation is determining appropriate spatial scopes based on satellite image resolution and junction patterns. Specifically, we first download OpenStreetMap data from areas with relatively high satellite image resolution and extract all junctions. We then manually review the corresponding satellite imagery from Google Maps² for each junction to eliminate invalid images that are fake, difficult to identify, or severely obscured, ultimately obtaining the final candidate bounding boxes. For FPV imagery, we extract valid instances from captured in-vehicle camera photos in the same junction candidates collected for the BEV tasks and road scenes from the same cities to ensure geographic consistency. For junction scene images used in lane counting and lane designation recognition, annotators are instructed to include a certain proportion of challenging scenarios, such as nighttime conditions or obscured lane markings, to test the capabilities of MLLMs. For road scenes, the number of images for main roads and service roads keep consistent to avoid class imbalance issues.

Data Processing. After completing data preparation, the bounding box data is fed into the database of the tier-1 online map service provider to extract labels such as actual road centerlines, junction locations, the number of lanes, and lane directions within the specified area. These high-quality datasets are directly applicable to lane-related tasks as ground truth. Meanwhile, when matched with OpenStreetMap data, they form inaccurate reference lines and ground truth pairs suitable for road network correction tasks. For FPV images captured at junction and road scenes, the required labels including lane count, lane direction type, and road type are matched from the map provider’s database by using the image capture coordinates. All datasets have undergone anonymization and privacy handling. All IDs have been randomized into UUIDs. All location coordinates have been processed into pixel coordinates on the images. All content in FPV images that could potentially expose the privacy of the photographer or the surrounding environment has been manually obscured using gray masks.

Quality Control. Due to the fact that certain steps involve automated program matching, a small number of annotation errors may occur. These errors can stem from factors such as coordinate inaccuracies and incorrect matching. To fully ensure dataset quality, all final test cases undergo a second round of manual proofreading via the LabelU annotation platform [25]. The rare erroneous or unrecognizable data were simply rejected rather than relabeled to avoid introducing manual errors.

²<https://www.google.com/maps>

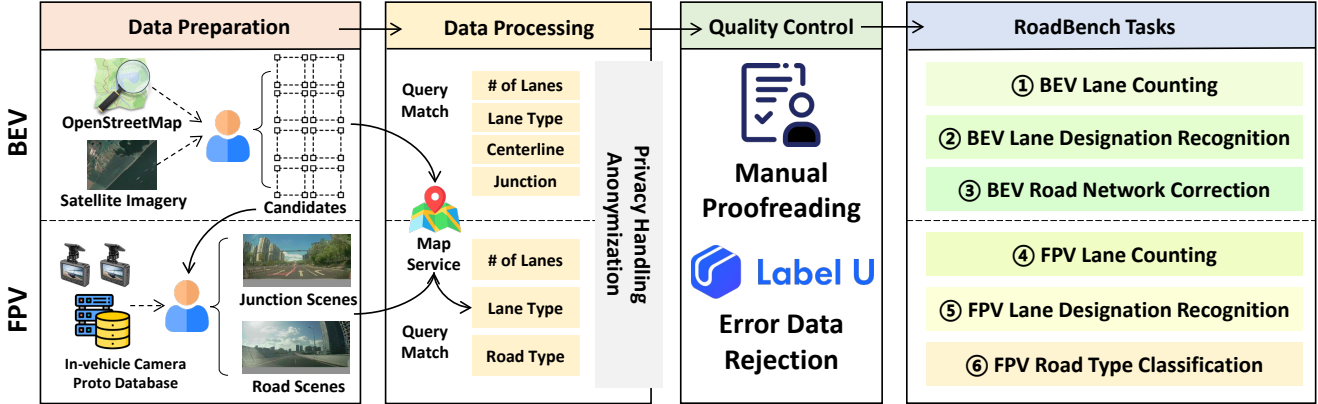


Figure 3. The RoadBench curation pipelines to construct the datasets for the six benchmark tasks.

4. Experiments

4.1. Evaluation Settings

Evaluated MLLMs. To comprehensively evaluate the performance of MLLMs on RoadBench, we selected mainstream MLLMs released within the last one year and included both open-source and closed-source models with varying parameter counts from different providers. In the open-source models, we selected the 11B and 90B versions of LLaMA-3.2-Vision, the 7B, 32B, and 72B versions of Qwen2.5-VL [3], the 12B and 27B versions of Gemma-3 [31], and GLM-4.5V [32]. In the closed-source model selection, we chose Gemini-2.5-Flash, Gemini-2.5-Flash-Image, Gemini-2.5-Pro from Google [9], as well as GPT-5-Nano, GPT-5-Mini, and GPT-5 from OpenAI.

Baselines. To aid in understanding the practical applicability of MLLM across these benchmark tasks, we include several rule-based or simple random baselines. In the two lane counting task, we provided two baselines: always choose two lanes and randomly select two lanes from $\{2, 3, 4\}$ with a uniform distribution. For the two lane designation recognition task, we designed a mapping table based on traffic common sense as a baseline. The details can be found in Appendix 7.2. The FPV road type classification task uses uniformly distributed random selection as the baseline. Due to the complexity of the BEV road network correction task, we directly treat the input reference line as the output road segment polyline, using the start and end points of the reference line as the coordinates of the identified intersection. The main result shown in Table 2 will only include the optimal baseline. Complete experimental results can be found in Appendix 7. In addition, since the Quality Control phase only retained data that could be correctly identified by a human, we believe that a human with the related knowledge can perform all tasks completely correctly. Therefore, no human baseline is provided for comparison.

Evaluation Metrics. Throughout the entire experiment,

the performance of MLLMs across various tasks was comprehensively evaluated using the metrics shown in Figure 2. The metrics (Precision, Recall, and F1-Score) used to evaluate multi-classification tasks are weighted according to the sample size. In the BEV road network correction task, the normalized distance upper bound thresholds for RMSE and Fréchet Distance were set to $\{10\%, 20\%, 50\%\}$ to ultimately select the appropriate threshold. Due to page size limitations, the main results in Table 2 report no more than two metrics that best reflect the performance of MLLMs. The complete results can be found in Appendix 7. Beyond these metrics, we use a composite ranking as an intuitive auxiliary metric to assess the overall relative performance of MLLMs. For each task, we sum the rankings on the two key metrics and sort the totals to obtain the final rank.

Error Handling. To minimize the interference of detectable errors on MLLMs’ fine-grained spatial understanding and reasoning evaluation, the benchmark procedure incorporates a series of error-handling mechanisms. The program detects issues such as failed API calls, empty response values, and incorrect return formats, and re-invokes MLLMs with identical inputs. This retry process is limited to a maximum of six attempts. If MLLMs still fail to produce correct results after retries, the outcome is recorded as zero or empty.

4.2. Main Results

The comprehensive evaluation results on RoadBench for the selected MLLMs and baselines are listed in Table 2. By analyzing these results, we can find the following conclusions.

RoadBench is a highly challenging benchmark for MLLMs. Overall, neither the most powerful closed-source models nor open-source models perform sufficiently well on the tasks proposed by RoadBench for evaluating the fine-grained understanding and reasoning capabilities of MLLMs in urban scenarios. For example, in the BEV lane counting task, the best model GPT-5-Mini achieved an F1-Score of only 0.369, and the RMSE between the predicted lane counts

Table 2. The comprehensive evaluation results on RoadBench. The best-performing result is indicated in **bold**, and the second-best one is indicated with an underline. In the table, F1, HL, and FD are abbreviations for F1-Score, Hamming Loss, and Fréchet Distance, respectively. For BEV road network correction tasks, the normalized distance upper threshold for the RMSE metric used to evaluate junction point accuracy is 20%, while the one for the Fréchet Distance metric used to evaluate segment polyline accuracy is 50%.

Model	BEV Lane Counting		BEV Lane Designation Recognition		BEV Road Network Correction		FPV Lane Counting		FPV Lane Designation Recognition		FPV Road Type Classification	Rank
	F1 ↑	RMSE ↓	HL ↓	Acc. ↑	RMSE ↓	FD ↓	F1 ↑	RMSE ↓	HL ↓	Acc. ↑	Acc. ↑	
LLaMA-3.2-11B-Vision	0.241	1.579	0.354	0.138	0.171	0.379	0.273	1.431	0.349	0.159	0.553	14
LLaMA-3.2-90B-Vision	0.295	1.334	0.207	0.470	0.149	0.307	0.305	1.138	0.161	0.525	0.640	6
Qwen2.5-VL-7B	0.241	1.409	0.296	0.103	0.170	0.398	0.221	1.416	0.287	0.167	0.530	13
Qwen2.5-VL-32B	0.280	1.243	0.226	0.384	0.154	0.313	0.335	1.088	0.232	0.323	0.563	11
Qwen2.5-VL-72B	0.205	1.342	0.204	0.477	<u>0.138</u>	0.259	0.317	1.201	0.181	0.481	0.595	7
Gemma-3-12B	0.222	1.194	0.250	0.349	0.159	0.298	0.220	1.206	0.237	0.364	0.575	12
Gemma-3-27B	0.279	1.331	0.205	0.415	0.143	0.232	0.271	1.206	0.202	0.404	0.524	10
Gemini-2.5-Flash	0.239	1.419	0.196	0.483	0.148	0.281	0.339	1.176	0.170	0.508	0.556	8
Gemini-2.5-Flash-Image	0.236	1.372	0.181	0.494	0.146	0.270	0.299	1.272	0.177	0.479	0.569	9
Gemini-2.5-Pro	<u>0.322</u>	1.250	0.164	0.537	0.144	0.293	<u>0.509</u>	<u>0.894</u>	0.143	0.569	0.764	3
GLM-4.5V	0.316	1.177	0.168	0.546	0.171	0.271	0.382	0.997	0.143	0.579	0.598	4
GPT-5-Nano	0.188	1.511	0.164	0.554	0.132	0.258	0.289	1.252	0.150	0.544	0.612	5
GPT-5-Mini	0.369	<u>1.151</u>	<u>0.152</u>	0.556	0.139	<u>0.241</u>	0.412	0.931	0.130	<u>0.594</u>	0.607	1
GPT-5	0.309	1.351	0.156	<u>0.586</u>	0.142	0.261	0.526	0.837	<u>0.129</u>	0.593	<u>0.705</u>	<u>2</u>
Rule-based	0.267	1.109	0.141	0.605	0.155	0.381	0.225	1.440	0.128	0.602	0.504	-

and the ground truth exceeded 1, reaching 1.151. This indicates that MLLMs fail to effectively and robustly understand the fine-grained spatial structure of road markings in images. Furthermore, the results of the BEV road network correction task indicate that MLLMs struggle to accurately provide coordinates for corrected intersections and road segments. The best model exhibits an RMSE@20% as high as 0.132 for junction points and an FD@50% as high as 0.232 for road segment polylines, both falling within the same order of magnitude as the upper threshold set. These results suggest that current MLLMs are unable to reason based on fine-grained spatial elements and complete tasks requiring global information and also fully demonstrate that RoadBench is a highly challenging benchmark.

MLLMs struggle to outperform simple rule-based methods that do not rely on any image inputs. Comparing against baselines based on simple rules is a better way to understand the above results than simply interpreting the absolute values of the outcome metrics. Observing the results of the two lane designation recognition tasks reveals that none of the MLLMs can outperform the baseline designed based on traffic domain common sense. Even in the BEV viewpoint, they exhibit a relative gap of approximately 7.8% in Hamming Loss and about 3.1% in accuracy compared to the baseline. In other scenarios except the FPV road

type classification task, some MLLMs also fail to outperform the baseline based on random choice. By comparing results against simple rules or random selections, we find that MLLMs still have significant room for improvement in fine-grained spatial understanding and the application of domain-specific common sense.

MLLMs struggle to provide precise coordinate numbers. The BEV road network correction task requires MLLMs to return coordinates for points and polylines based on their understanding and reasoning of the input. By examining the metrics shown in Table 73 at the small threshold (10%), we observe that the results are almost entirely contributed by the distance upper threshold. This indicates that the points or lines generated by MLLMs shift significantly from the ground truth, reflecting their limitations in spatial understanding and reasoning, or in the accuracy of structured numerical outputs.

MLLMs are better at correctly understanding the fine-grained spatial elements contained within FPV images. Comparing the results of the same task under FPV and BEV viewpoints, we observe that MLLMs demonstrate significantly superior performance on FPV images compared to BEV images, both in terms of absolute metric values and relative gaps compared to the baseline. This indicates that larger spatial elements such as road markings and signs in

the FPV viewpoint can be better understood by MLLMs. Conversely, it also reflects the limitations of MLLMs in understanding more granular spatial elements in BEV images.

The number of parameters is not a universal solution in RoadBench. Although the number of parameters is largely positively correlated with the capabilities of MLLMs, larger models do not necessarily perform better. For example, GPT-5-Mini outperforms GPT-5 on most tasks. Qwen2.5-VL-32B also outperformed Qwen2.5-VL-72B in the FPV lane recognition task. This may be related to the fusion method or training process of the visual and textual modalities within MLLMs.

Closed-source models hold certain technical advantages on RoadBench. From an overall ranking perspective, in terms of fine-grained spatial understanding capabilities within urban scenarios, closed-source models represented by the GPT-5 series (Rank 1, 2, and 5) and Gemini-2.5 series (Rank 3) have achieved certain technical advantages over open-source models. Among open-source models, only GLM-4.5V (Rank 4) ranks highly in comprehensive evaluations.

4.3. Further Analysis

The impact of reference line prompting methods in the BEV tasks. Since reference lines serve as the primary source for MLLMs to identify regions of interest in BEV tasks, how their positions are prompted to MLLMs may directly impact the task performance of MLLMs. We selected the closed-source model GPT-5-Mini and the open-source model GLM-4.5V, which demonstrated better performance in the BEV lane counting task and the BEV lane designation recognition task for further testing. We design different reference line prompt methods, including text-only prompts, visual-only prompts, and both text and visual prompts. Visual prompts are categorized into two approaches: using start and end point colors to indicate direction, and employing arrows on the line segments to denote direction. Both text and visual prompts with arrows are the default settings in the BEV tasks.

Based on the experimental results presented in Table 87 and Table 88, we observe significant differences in preference for prompt formats among various MLLMs, potentially attributable to variations in the data distribution used during training. GLM-4.5V shows a stronger tendency to learn from both textual prompts and image prompts with arrows, with image prompts playing a dominant role. When deprived of image prompts, GLM-4.5V’s performance declines by 1.24% to 15.04%, whereas losing textual prompts only causes performance fluctuations of 0.64% to 2.29%. GPT-5-Mini shows a stronger preference for prompts that use color to distinguish directions, while variations in prompting methods produce no more than a 4% deviation in the BEV lane designation recognition task. These phenomena

may indicate that GPT-5-Mini is better equipped to integrate textual and visual information to collaboratively process the entire information flow.

The impact of scene environment conditions in the FPV tasks. FPV images captured from in-vehicle cameras encompass varying external environmental conditions. Among these, the most direct factors affecting MLLM understanding and reasoning are adverse lighting conditions and obscured road markings. Regarding obscured road markings, only images where lane information could be determined through alternative means were retained during manual dataset proofreading. After additional annotation, 175 test cases involving adverse lighting conditions were identified, alongside 46 test cases featuring obscured road markings. To analyze the impact of different scenario environments on MLLMs, we selected GLM-4.5V, GPT-5, and Gemini-2.5-Pro which performed well in the main results as case studies.

The experimental results in the FPV lane counting task and the FPV lane designation recognition task are presented in Table 89, Table 810 and Table 811. Based on the results, we have two primary findings. First, adverse lighting conditions do indeed degrade the performance of MLLMs, but this impact is significantly alleviated in models with strong image understanding and reasoning capabilities. For example, for GPT-5, adverse lighting conditions only caused a 0.2%-1.9% drop in performance. Second, shifting the basis for task completion from obscured road markings to other elements like signage substantially improved the performance of both GPT-5 and Gemini-2.5-Pro. This phenomenon indicates that MLLMs exhibit significantly weaker capabilities in understanding and reasoning fine-grained spatial elements compared to other capabilities.

5. Conclusion

In this paper, we propose a benchmark named RoadBench with six benchmark tasks and 9,121 test cases for comprehensively evaluating MLLMs’ understanding and reasoning of fine-grained spatial elements under urban scenarios based on both BEV and FPV images. Based on this benchmark, we evaluated 14 mainstream MLLMs. The results and further analysis indicate that existing MLLMs lack proper fine-grained spatial understanding and reasoning capabilities under urban scenarios. On certain tasks and metrics, they even fail to outperform baselines based on random selection or simple rules. These findings indicate the significance of RoadBench while also highlighting the need to enhance MLLM’s capabilities in fine-grained spatial understanding and reasoning. Based on this fact, RoadBench is promising to become the foundational dataset and evaluation framework for advancing research and applications that enhance the fine-grained spatial understanding and reasoning capabilities of MLLM or MLLM-based agents.

References

- [1] Josh Achiam, Steven Adler, Sandhini Agarwal, Lama Ahmad, Ilge Akkaya, Florencia Leoni Aleman, Diogo Almeida, Janko Altenschmidt, Sam Altman, Shyamal Anadkat, et al. Gpt-4 technical report. *arXiv preprint arXiv:2303.08774*, 2023. 1, 2
- [2] Alisson Azzolini, Junjie Bai, Hannah Brandon, Jiaxin Cao, Prithvijit Chattopadhyay, Huayu Chen, Jinju Chu, Yin Cui, Jenna Diamond, Yifan Ding, et al. Cosmos-reason1: From physical common sense to embodied reasoning. *arXiv preprint arXiv:2503.15558*, 2025. 2
- [3] Shuai Bai, Keqin Chen, Xuejing Liu, Jialin Wang, Wenbin Ge, Sibao Song, Kai Dang, Peng Wang, Shijie Wang, Jun Tang, et al. Qwen2. 5-vl technical report. *arXiv preprint arXiv:2502.13923*, 2025. 1, 2, 6
- [4] Tom Brown, Benjamin Mann, Nick Ryder, Melanie Subbiah, Jared D Kaplan, Prafulla Dhariwal, Arvind Neelakantan, Pranav Shyam, Girish Sastry, Amanda Askell, et al. Language models are few-shot learners. *Advances in neural information processing systems*, 33:1877–1901, 2020. 2
- [5] Xinyuan Chang, Maixuan Xue, Xinran Liu, Zheng Pan, and Xing Wei. Driving by the rules: A benchmark for integrating traffic sign regulations into vectorized hd map. In *Proceedings of the Computer Vision and Pattern Recognition Conference*, pages 6823–6833, 2025. 3, 4
- [6] Boyuan Chen, Zhuo Xu, Sean Kirmani, Brian Ichter, Dorsa Sadigh, Leonidas Guibas, and Fei Xia. SpatialVlm: Endowing vision-language models with spatial reasoning capabilities. In *Proceedings of the IEEE/CVF Conference on Computer Vision and Pattern Recognition*, pages 14455–14465, 2024. 2
- [7] Jiabin Chen, Haiping Wang, Jinpeng Li, Yuan Liu, Zhen Dong, and Bisheng Yang. Spatialllm: From multimodality data to urban spatial intelligence. *arXiv preprint arXiv:2505.12703*, 2025. 3
- [8] An-Chieh Cheng, Hongxu Yin, Yang Fu, Qiushan Guo, Ruihan Yang, Jan Kautz, Xiaolong Wang, and Sifei Liu. Spatialrgpt: Grounded spatial reasoning in vision-language models. *Advances in Neural Information Processing Systems*, 37: 135062–135093, 2024. 2
- [9] Gheorghe Comanici, Eric Bieber, Mike Schaekermann, Ice Pasupat, Naveen Sachdeva, Inderjit Dhillon, Marcel Bliestein, Ori Ram, Dan Zhang, Evan Rosen, et al. Gemini 2.5: Pushing the frontier with advanced reasoning, multimodality, long context, and next generation agentic capabilities. *arXiv preprint arXiv:2507.06261*, 2025. 6
- [10] Can Cui, Yunsheng Ma, Xu Cao, Wenqian Ye, Yang Zhou, Kaizhao Liang, Jintai Chen, Juanwu Lu, Zichong Yang, Kueida Liao, et al. A survey on multimodal large language models for autonomous driving. In *Proceedings of the IEEE/CVF winter conference on applications of computer vision*, pages 958–979, 2024. 1, 2
- [11] Erik Daxberger, Nina Wenzel, David Griffiths, Haiming Gang, Justin Lazarow, Gefen Kohavi, Kai Kang, Marcin Eichner, Yinfei Yang, Afshin Dehghan, et al. Mm-spatial: Exploring 3d spatial understanding in multimodal llms. In *Proceedings of the IEEE/CVF International Conference on Computer Vision*, pages 7395–7408, 2025. 3
- [12] Danny Driess, Fei Xia, Mehdi SM Sajjadi, Corey Lynch, Aakanksha Chowdhery, Brian Ichter, Ayzaan Wahid, Jonathan Tompson, Quan Vuong, Tianhe Yu, et al. Palm-e: An embodied multimodal language model. In *International Conference on Machine Learning*, pages 8469–8488. PMLR, 2023. 1
- [13] Thomas Eiter, Heikki Mannila, et al. Computing discrete fréchet distance. 1994. 4
- [14] Jie Feng, Tianhui Liu, Yuwei Du, Siqi Guo, Yuming Lin, and Yong Li. Citygpt: Empowering urban spatial cognition of large language models. In *Proceedings of the 31st ACM SIGKDD Conference on Knowledge Discovery and Data Mining V. 2*, pages 591–602, 2025. 1, 3
- [15] Jie Feng, Shengyuan Wang, Tianhui Liu, Yanxin Xi, and Yong Li. Urbanllava: A multi-modal large language model for urban intelligence with spatial reasoning and understanding. In *Proceedings of the IEEE/CVF International Conference on Computer Vision*, pages 6209–6219, 2025. 1, 3
- [16] Jie Feng, Jun Zhang, Tianhui Liu, Xin Zhang, Tianjian Ouyang, Junbo Yan, Yuwei Du, Siqi Guo, and Yong Li. Citybench: Evaluating the capabilities of large language models for urban tasks. In *Proceedings of the 31st ACM SIGKDD Conference on Knowledge Discovery and Data Mining V. 2*, pages 5413–5424, 2025. 1, 3, 4
- [17] Chaoyou Fu, Peixian Chen, Yunhang Shen, Yulei Qin, Mengdan Zhang, Xu Lin, Jinrui Yang, Xiawu Zheng, Ke Li, Xing Sun, Yunsheng Wu, and Rongrong Ji. Mme: A comprehensive evaluation benchmark for multimodal large language models, 2024. 3
- [18] Qiushan Guo, Shalini De Mello, Hongxu Yin, Wonmin Byeon, Ka Chun Cheung, Yizhou Yu, Ping Luo, and Sifei Liu. Regiongpt: Towards region understanding vision language model. In *Proceedings of the IEEE/CVF Conference on Computer Vision and Pattern Recognition*, pages 13796–13806, 2024. 2
- [19] Huiyang Hu, Peijin Wang, Hanbo Bi, Boyuan Tong, Zhaozhi Wang, Wenhui Diao, Hao Chang, Yingchao Feng, Ziqi Zhang, Yaowei Wang, et al. Rs-vheat: Heat conduction guided efficient remote sensing foundation model. In *Proceedings of the IEEE/CVF International Conference on Computer Vision*, pages 9876–9887, 2025. 3
- [20] Bohao Li, Yuying Ge, Yixiao Ge, Guangzhi Wang, Rui Wang, Ruimao Zhang, and Ying Shan. Seed-bench: Benchmarking multimodal large language models. In *Proceedings of the IEEE/CVF Conference on Computer Vision and Pattern Recognition*, pages 13299–13308, 2024. 3
- [21] Junnan Li, Dongxu Li, Caiming Xiong, and Steven Hoi. Blip: Bootstrapping language-image pre-training for unified vision-language understanding and generation. In *International conference on machine learning*, pages 12888–12900. PMLR, 2022. 2
- [22] Xiaoqi Li, Mingxu Zhang, Yiran Geng, Haoran Geng, Yuxing Long, Yan Shen, Renrui Zhang, Jiaming Liu, and Hao Dong. Manipllm: Embodied multimodal large language model for object-centric robotic manipulation. In *Proceedings of the IEEE/CVF Conference on Computer Vision and Pattern Recognition*, pages 18061–18070, 2024. 1
- [23] Yuan Liu, Haodong Duan, Yuanhan Zhang, Bo Li, Songyang Zhang, Wangbo Zhao, Yike Yuan, Jiaqi Wang, Conghui He,

- Ziwei Liu, et al. Mmbench: Is your multi-modal model an all-around player? In *European conference on computer vision*, pages 216–233. Springer, 2024. 3
- [24] Pan Lu, Hritik Bansal, Tony Xia, Jiacheng Liu, Chunyuan Li, Hannaneh Hajishirzi, Hao Cheng, Kai-Wei Chang, Michel Galley, and Jianfeng Gao. Mathvista: Evaluating mathematical reasoning of foundation models in visual contexts. *arXiv preprint arXiv:2310.02255*, 2023. 2
- [25] OpenDataLab. Labelu, 2025. Accessed: 2025-09-01. 5
- [26] Ruizhe Ou, Yuan Hu, Fan Zhang, Jiabin Chen, and Yu Liu. Geopix: A multimodal large language model for pixel-level image understanding in remote sensing. *IEEE Geoscience and Remote Sensing Magazine*, 2025. 2, 3
- [27] Sung-Yeon Park, Can Cui, Yunsheng Ma, Ahmadreza Moradipari, Rohit Gupta, Kyungtae Han, and Ziran Wang. Nuplanqa: A large-scale dataset and benchmark for multi-view driving scene understanding in multi-modal large language models. *arXiv preprint arXiv:2503.12772*, 2025. 3, 4
- [28] Alec Radford, Jong Wook Kim, Chris Hallacy, Aditya Ramesh, Gabriel Goh, Sandhini Agarwal, Girish Sastry, Amanda Askell, Pamela Mishkin, Jack Clark, et al. Learning transferable visual models from natural language supervision. In *International conference on machine learning*, pages 8748–8763. PmLR, 2021. 2
- [29] Santhosh Kumar Ramakrishnan, Erik Wijmans, Philipp Kraehenbuehl, and Vladlen Koltun. Does spatial cognition emerge in frontier models? *arXiv preprint arXiv:2410.06468*, 2024. 3
- [30] Jonathan Roberts, Timo Lüddecke, Rehan Sheikh, Kai Han, and Samuel Albanie. Charting new territories: Exploring the geographic and geospatial capabilities of multimodal llms. In *Proceedings of the IEEE/CVF Conference on Computer Vision and Pattern Recognition*, pages 554–563, 2024. 1
- [31] Gemma Team, Aishwarya Kamath, Johan Ferret, Shreya Pathak, Nino Vieillard, Ramona Merhej, Sarah Perrin, Tatiana Matejovicova, Alexandre Ramé, Morgane Rivière, et al. Gemma 3 technical report. *arXiv preprint arXiv:2503.19786*, 2025. 1, 2, 6
- [32] V Team, Wenyi Hong, Wenmeng Yu, Xiaotao Gu, Guo Wang, Guobing Gan, Haomiao Tang, Jiale Cheng, Ji Qi, Junhui Ji, Lihang Pan, Shuaiqi Duan, Weihang Wang, Yan Wang, Yean Cheng, Zehai He, Zhe Su, Zhen Yang, Ziyang Pan, Aohan Zeng, Baoxu Wang, Bin Chen, Boyan Shi, Changyu Pang, Chenhui Zhang, Da Yin, Fan Yang, Guoqing Chen, Jiazheng Xu, Jiale Zhu, Jiali Chen, Jing Chen, Jinhao Chen, Jinghao Lin, Jinjiang Wang, Junjie Chen, Leqi Lei, Letian Gong, Leyi Pan, Mingdao Liu, Mingde Xu, Mingzhi Zhang, Qinkai Zheng, Sheng Yang, Shi Zhong, Shiyu Huang, Shuyuan Zhao, Siyan Xue, Shangqin Tu, Shengbiao Meng, Tianshu Zhang, Tianwei Luo, Tianxiang Hao, Tianyu Tong, Wenkai Li, Wei Jia, Xiao Liu, Xiaohan Zhang, Xin Lyu, Xinyue Fan, Xuancheng Huang, Yanling Wang, Yadong Xue, Yanfeng Wang, Yanzi Wang, Yifan An, Yifan Du, Yiming Shi, Yiheng Huang, Yilin Niu, Yuan Wang, Yuanchang Yue, Yuchen Li, Yutao Zhang, Yuting Wang, Yu Wang, Yuxuan Zhang, Zhao Xue, Zhenyu Hou, Zhengxiao Du, Zihan Wang, Peng Zhang, Debing Liu, Bin Xu, Juanzi Li, Minlie Huang, Yuxiao Dong, and Jie Tang. Glm-4.5v and glm-4.1v-thinking: Towards versatile multimodal reasoning with scalable reinforcement learning, 2025. 6
- [33] Xiaoyu Tian, Junru Gu, Bailin Li, Yicheng Liu, Yang Wang, Zhiyong Zhao, Kun Zhan, Peng Jia, XianPeng Lang, and Hang Zhao. Drivevlm: The convergence of autonomous driving and large vision-language models. In *Conference on Robot Learning*, pages 4698–4726. PMLR, 2025. 1
- [34] Hugo Touvron, Thibaut Lavril, Gautier Izacard, Xavier Martinet, Marie-Anne Lachaux, Timothée Lacroix, Baptiste Rozière, Naman Goyal, Eric Hambro, Faisal Azhar, et al. Llama: Open and efficient foundation language models. *arXiv preprint arXiv:2302.13971*, 2023. 2
- [35] Jiayu Wang, Yifei Ming, Zhenmei Shi, Vibhav Vineet, Xin Wang, Sharon Li, and Neel Joshi. Is a picture worth a thousand words? delving into spatial reasoning for vision language models. *Advances in Neural Information Processing Systems*, 37:75392–75421, 2024. 3
- [36] Xingrui Wang, Wufei Ma, Tiezheng Zhang, Celso M de Melo, Jieneng Chen, and Alan Yuille. Spatial457: A diagnostic benchmark for 6d spatial reasoning of large multimodal models. In *Proceedings of the Computer Vision and Pattern Recognition Conference*, pages 24669–24679, 2025. 3
- [37] Haoran Wei, Youyang Yin, Yumeng Li, Jia Wang, Liang Zhao, Jianjian Sun, Zheng Ge, Xiangyu Zhang, and Daxin Jiang. Slow perception: Let’s perceive geometric figures step-by-step. *arXiv preprint arXiv:2412.20631*, 2024. 2
- [38] Hanguang Xiao, Feizhong Zhou, Xingyue Liu, Tianqi Liu, Zhipeng Li, Xin Liu, and Xiaoxuan Huang. A comprehensive survey of large language models and multimodal large language models in medicine. *Information Fusion*, page 102888, 2024. 2
- [39] Shaoyuan Xie, Lingdong Kong, Yuhao Dong, Chonghao Sima, Wenwei Zhang, Qi Alfred Chen, Ziwei Liu, and Liang Pan. Are vlms ready for autonomous driving? an empirical study from the reliability, data, and metric perspectives. *arXiv preprint arXiv:2501.04003*, 2025. 1, 3, 4
- [40] Weihao Xuan, Junjue Wang, Heli Qi, Zihang Chen, Zhuo Zheng, Yanfei Zhong, Junshi Xia, and Naoto Yokoya. Dynamicvl: Benchmarking multimodal large language models for dynamic city understanding. *arXiv preprint arXiv:2505.21076*, 2025. 3
- [41] Jihan Yang, Shusheng Yang, Anjali W Gupta, Rilyn Han, Li Fei-Fei, and Saining Xie. Thinking in space: How multimodal large language models see, remember, and recall spaces. In *Proceedings of the Computer Vision and Pattern Recognition Conference*, pages 10632–10643, 2025. 3
- [42] Shukang Yin, Chaoyou Fu, Sirui Zhao, Ke Li, Xing Sun, Tong Xu, and Enhong Chen. A survey on multimodal large language models. *National Science Review*, 11(12):nwae403, 2024. 1, 2
- [43] Ruifei Zhang, Wei Zhang, Xiao Tan, Sibe Yang, Xiang Wan, Xiaonan Luo, and Guanbin Li. Vldrive: Vision-augmented lightweight mllms for efficient language-grounded autonomous driving. In *Proceedings of the IEEE/CVF International Conference on Computer Vision*, pages 5923–5933, 2025. 3
- [44] Shan Zhang, Aotian Chen, Yanpeng Sun, Jindong Gu, Yi-Yu Zheng, Piotr Koniusz, Kai Zou, Anton van den Hengel,

- and Yuan Xue. Open eyes, then reason: Fine-grained visual mathematical understanding in mllms. *arXiv preprint arXiv:2501.06430*, 2025. 2
- [45] Wei Zhang, Miaoxin Cai, Tong Zhang, Yin Zhuang, Jun Li, and Xuerui Mao. Earthmarker: A visual prompting multi-modal large language model for remote sensing. *IEEE Transactions on Geoscience and Remote Sensing*, 2024. 1
- [46] Xin Zhang, Tianjian Ouyang, Yu Shang, Qingmin Liao, and Yong Li. Urbanmllm: Joint learning of cross-view imagery for urban understanding. 2025. 1
- [47] Ye Zhang and Yiming Nie. Interndrive: A multimodal large language model for autonomous driving scenario understanding. In *Proceedings of the 2024 4th International Conference on Artificial Intelligence, Automation and High Performance Computing*, pages 294–305, 2024. 1
- [48] Baining Zhao, Ziyou Wang, Jianjie Fang, Chen Gao, Fanhang Man, Jinqiang Cui, Xin Wang, Xinlei Chen, Yong Li, and Wenwu Zhu. Embodied-r: Collaborative framework for activating embodied spatial reasoning in foundation models via reinforcement learning. In *Proceedings of the 33rd ACM International Conference on Multimedia*, pages 11071–11080, 2025. 3
- [49] Yong Zhao, Kai Xu, Zhengqiu Zhu, Yue Hu, Zhiheng Zheng, Yingfeng Chen, Yatai Ji, Chen Gao, Yong Li, and Jincan Huang. Cityeqa: A hierarchical llm agent on embodied question answering benchmark in city space. *EMNLP*, 2025. 3, 4
- [50] Baichuan Zhou, Haote Yang, Dairong Chen, Junyan Ye, Tianyi Bai, Jinhua Yu, Songyang Zhang, Dahua Lin, Conghui He, and Weijia Li. Urbench: A comprehensive benchmark for evaluating large multimodal models in multi-view urban scenarios. In *Proceedings of the AAAI Conference on Artificial Intelligence*, pages 10707–10715, 2025. 1, 3, 4

RoadBench: Benchmarking MLLMs on Fine-Grained Spatial Understanding and Reasoning under Urban Road Scenarios

Supplementary Material

We present the following items in the appendix section:

1. The prompts of all the 6 benchmark tasks. (Section 6)
2. Additional experimental setup descriptions and complete results. (Section 7)
3. Two results supporting further analysis about the impact of reference line prompting methods in the BEV tasks and the impact of scene environment conditions in the FPV tasks. (Section 8)
4. Analysis of failure cases in all the 6 benchmark tasks. (Section 9)

6. Prompts of Benchmark Tasks

Examples of prompts for each task in RoadBench and typical MLLM responses are listed below. It is worth noting that in the prompt design for RoadBench, the requirement for MLLM to return YAML format with a line of comments balances the need for explicit reasoning with the demand for structured output.

6.1. BEV Lane Counting

An example image (Figure 61) and prompt of the BEV lane counting task are as follows:



Figure 61. An example image input to MLLM in the BEV lane counting task.

Task: Lane Counting for Road Network Analysis

Image Description: This is a satellite image of a road network in China, where vehicles drive on the right side of the road. A specific road segment has been marked as a red polyline with arrowheads.

Data:

```
```yaml
The image size
image:
 width: 910
 height: 779
The pixel coordinates of the
 reference centerline
coordinates:
- x: 510.0
 y: 778.0
- x: 400.0
 y: 400.0
```
```

Question: Analyze the marked road segment and determine: How many lanes are available for vehicles traveling in the direction of the arrow?

YAML Output Requirements:

- Add ONLY one-line YAML comment explaining your visual analysis and reasoning
- Extract num_lanes (integer)

Output Format:

```
```yaml
Explanation: [Describe what you see
 that led to your determination]
num_lanes: <integer>
```
```

Your YAML output:

Typical MLLM responses for the image and prompt are as follows:

Response from GPT-5:

```
```yaml
Explanation: On the right half of
 the divided roadway (arrow
 direction), there are three clearly
 marked lanes separated by dashed
 white lines between the curb and
 the central median.
num_lanes: 3
```
```

```

'''
Response from Qwen2.5-7B-instruct:
```yaml
Explanation: Observing from top-down
view, there appear three distinct
parallel lines indicating separate
traffic lanes.
num_lanes: 3
'''

```

## 6.2. BEV Lane Designation Recognition

An example image (Figure 62) and prompt of the BEV lane designation recognition task are as follows:



Figure 62. An example image input to MLLM in the BEV lane designation recognition task.

### Task: Lane Designations Recognition for Road Network Analysis

**Image Description:** This is a satellite image of a road network in China, where vehicles drive on the right side of the road. A specific road segment has been marked as a red polyline with arrowheads.

**Data:**

```

```yaml
# The number of lanes

```

```

num_lanes: 3
# The image size
image:
  width: 899
  height: 1054
# The pixel coordinates of the
reference centerline
coordinates:
- x: 499.0
  y: 714.0
- x: 400.0
  y: 400.0
'''

```

Question: Analyze the marked road segment and determine: What are the lane designations in the direction of the arrow?

Lane Direction Types: The available lane direction types include:

- (1) U-turn
- (2) left-turn
- (3) straight
- (4) right-turn

YAML Output Requirements:

- Add ONLY one-line YAML comment explaining your visual analysis and reasoning
- Return `lane_designations` as a list where each item represents the lane direction types for each lane from left to right
 - Make sure the number of lane designations is equal to the number of lanes (which is 3)
- Each lane can have multiple direction types, so each item in the list should also be a list
- Use the English terms: "U-turn", "left-turn", "straight", "right-turn"

Output Format:

```

```yaml
Explanation: [Describe what you see
that led to your determination]
lane_designations: [{"direction1", "
direction2"}, {"direction3"}, ...]
'''

```

Your YAML output:

Typical MLLM responses for the image and prompt are as follows:

**Response from GPT-5-mini:**

```

Explanation: Pavement arrow markings
show a dedicated left-turn lane on
the left, a straight-only center

```

```

line, and a rightmost lane marked
for both straight and right turns
lane_designations: [{"left-turn"}, {"
straight"}, {"straight", "right-
turn"}]]

```

**Response from Google Gemini-2.5-Flash:**

```

```yaml
# Explanation: From the bottom of the
marked segment, the leftmost lane
has a straight arrow and a right-
turn arrow. The middle lane has a
straight arrow. The rightmost lane
has a straight arrow.
lane_designations: [{"straight", "
right-turn"}, {"straight"}, {"
straight"}]]
```

```

### 6.3. BEV Road Network Correction

An example image (Figure 63) and prompt of the BEV road network correction task are as follows:

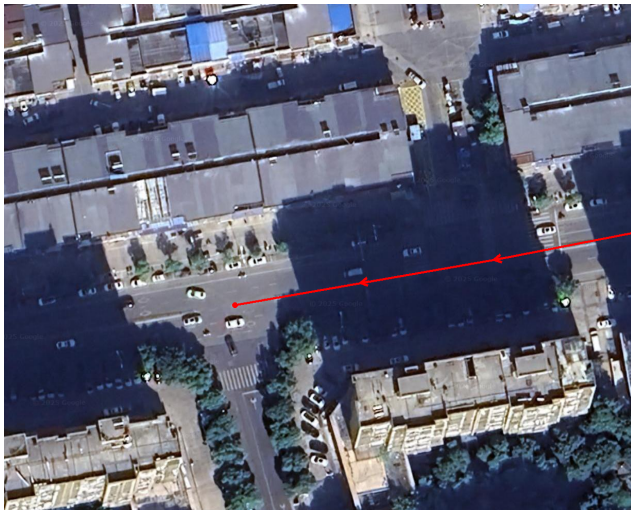


Figure 63. An example image input to MLLM in the BEV road network correction task.

**Task: Road Network Modification and Junction Identification**

**Image Description:** This is a satellite image of a road network in China, where vehicles drive on the right side of the road. A reference line has been marked as a red directed polyline to indicate the path and direction of travel along a road.

**Data:**

```

```yaml
# The image size
image:
  width: 1225
  height: 984
# The pixel coordinates of the
reference centerline
coordinates:
- x: 1225.0
  y: 443.0
- x: 958.0
  y: 495.0
- x: 448.0
  y: 584.0
```

```

**Task Description:** The given reference line may have missed important junctions such as intersections, highway on/off ramps, U-turn locations, dedicated right-turn lanes, etc., and it may not always be accurately aligned with the true centerline of the road. Your task is to analyze the image and identify:

- Junctions:** Important road intersections, merging points, or decision points that should be marked. Junctions are represented by WKT POINT geometries.
- Line Segments (with Directionality):** Road segments between junctions that represent the centerlines of the roads, with attention to the direction of travel (from start to end, following the reference line's direction). Line segments are represented by WKT LINESTRING geometries, and their order and orientation should reflect the actual direction of traffic flow along the road.

**Analysis Requirements:**

- Carefully examine the directed reference line and the actual road network in the image
- Identify any missing junctions where the directed reference line should be split (intersections, ramps, etc.)
- Return corrected directed line segments that represent the centerlines between identified junctions
- Ensure junctions are placed at the center points of intersections/decision points
- Ensure line segments follow the actual road centerlines
- Do not return junctions or line segments that are not related to the directed reference line

**YAML Output Requirements:**

- Add ONLY one-line YAML comment explaining your analysis and corrections
- Return junctions as a list of WKT POINT geometries representing junction center points

- Return lines as a list of directed WKT LINESTRING geometries representing road centerlines between junctions
- Use pixel coordinates in the format: "POINT (x y)" and "LINESTRING (x1 y1, x2 y2, ...)"

**Output Format:**

```
```yaml
# Explanation: [Describe the junctions
  and line segments you identified
  and any corrections made to the
  directed reference line]
junctions: ["POINT (x1 y1)", "POINT (
  x2 y2)", ...]
lines: ["LINESTRING (x1 y1, x2 y2)", "
  LINESTRING (x2 y2, x3 y3)", ...]
```
```

Your YAML output:

Typical MLLM responses for the image and prompt are as follows:

**Response from Qwen2.5-VL-72B-instruct:**

```
```yaml
# Explanation: The reference line was
  extended to include a missed
  junction at the intersection and
  corrected to follow the road
  centerline accurately.
junctions: ["POINT (1225 443)", "POINT
  (958 495)", "POINT (700 550)", "
  POINT (448 584)"]
lines: ["LINESTRING (1225 443, 958
  495)", "LINESTRING (958 495, 700
  550)", "LINESTRING (700 550, 448
  584)"]
```
```

**Response from Llama-3.2-11B-vision-instruct:**

```
Explanation: Corrected and completed
 the directed reference line,
 identifying all junctions and
 centerlines between them, ensuring
 accurate representation of the road
 network in China.

junctions: ["POINT (958.0 495.0)", "
 POINT (448.0 584.0)", "POINT
 (1225.0 443.0)"]
lines: ["LINESTRING (1225.0 443.0,
 958.0 495.0)", "LINESTRING (958.0
 495.0, 448.0 584.0)", "LINESTRING
 (448.0 584.0, 1225.0 443.0)"]
```

**6.4. FPV Lane Counting**

An example image (Figure 64) and prompt of the FPV lane counting task are as follows:



Figure 64. An example image input to MLLM in the FPV lane counting task.

**Task: Lane Counting for Road Network Analysis**

**Image Description:** This is a personal viewpoint image of a road in China, where vehicles drive on the right side of the road.

**Question:** Analyze the image and determine: How many lanes are available for vehicles traveling in the direction of the road?

**YAML Output Requirements:**

- Add ONLY one-line YAML comment explaining your visual analysis and reasoning
- Extract num\_lanes (integer)

**Output Format:**

```
```yaml
# Explanation: [Describe what you see
  that led to your determination]
num_lanes: <integer>
```
```

Your YAML output:

Typical MLLM responses for the image and prompt are as follows:

**Response from Llama-3.2-90B-vision-instruct:**

```
```yaml
# The image shows a road with a clear
  division of lanes through white
  markings, indicating three distinct
  lanes for vehicles to travel in
  the direction shown.
num_lanes: 3
```
```

### Response from Qwen2.5-VL-7B-instruct:

```
```yaml
# Explanation: The image shows two
  solid white lines marking separate
  travel paths.
num_lanes: 2
```
```

## 6.5. FPV Lane Designation Recognition

An example image (Figure 65) and prompt of the FPV lane designation recognition task are as follows:



Figure 65. An example image input to MLLM in the FPV lane designation recognition task.

### Task: Lane Designations Recognition for Road Network Analysis

**Image Description:** This is a personal viewpoint image of a road in China, where vehicles drive on the right side of the road.

#### Data:

```
```yaml
# The number of lanes
num_lanes: 2
```
```

**Question:** Analyze the image and determine: What are the lane designations in the direction of the road?

**Lane Direction Types:** The available lane direction types include:

- (1) U-turn
- (2) left-turn
- (3) straight
- (4) right-turn
- (5) variable

#### YAML Output Requirements:

- Add ONLY one-line YAML comment explaining your visual analysis and reasoning
- Return `lane_designations` as a list where

each item represents the lane direction types for each lane from left to right

- Make sure the number of lane designations is equal to the number of lanes (which is 2)

- Each lane can have multiple direction types, so each item in the list should also be a list
- Use the English terms: "U-turn", "left-turn", "straight", "right-turn", "variable"

#### Output Format:

```
```yaml
# Explanation: [Describe what you see
  that led to your determination]
lane_designations: [{"direction1", "
  direction2"}, {"direction3"}, ...]
```
```

Your YAML output:

Typical MLLM responses for the image and prompt are as follows:

### Response from GLM-4.5V:

```
```yaml
# Explanation: The image shows a road
  with two lanes; the visible lane
  marking indicates a straight
  direction, and there are no other
  directional markings (like left-
  turn or right-turn arrows) for
  either lane, so both lanes are
  designated for straight travel.
lane_designations: [{"straight"}, {"
  straight"}]
```
```

### Response from GPT-5-nano:

```
Explanation: The two lanes ahead
 have forward (straight) arrow
 markings with no visible left/right
 /U-turn arrows, indicating straight
 travel for both lanes
lane_designations: [{"straight"}, {"
 straight"}]
```

## 6.6. FPV Road Type Classification

An example image (Figure 66) and prompt of the FPV road type classification task are as follows:

### Task: Road Type Classification

**Image Description:** This is a personal viewpoint image of a road in China, where vehicles drive on the



Figure 66. An example image input to MLLM in the FPV road type classification task.

right side of the road.

**Question:** Analyze the image and determine: Is the current vehicle traveling on a main road or a service road?

**Road Type Definitions:**

- **Main road:** Primary traffic arteries, highways, major streets with higher traffic capacity and speed limits
- **Service road:** Secondary roads, access roads, frontage roads, or auxiliary roads that typically serve adjacent properties or provide access to main roads

**YAML Output Requirements:**

- Add ONLY one-line YAML comment explaining your visual analysis and reasoning
- Extract `road_type` as either "main" or "service"

**Output Format:**

```
```yaml
# Explanation: [Describe what you see
    that led to your determination]
road_type: <"main" or "service">
```
```

Your YAML output:

Typical MLLM responses for the image and prompt are as follows:

**Response from Qwen2.5-VL-32B-instruct:**

```
```yaml
# Explanation: The presence of
    multiple lanes for vehicular
    movement, clear lane markings, and
    an elevated structure (likely part
    of a highway overpass) suggest this
```

```
    is a primary roadway designed for
    high-capacity traffic flow.
road_type: main
```
```

**Response from Gemma-3-12B-it:**

```
```yaml
# The presence of multiple lanes, a
    highway overpass, distinct
    separation from adjacent buildings,
    and steady vehicle flow suggest
    this is a main road.
road_type: main
```
```

## 7. Additional Experimental Setup Descriptions and Complete Results

### 7.1. BEV Lane Counting

The complete experimental results for the BEV lane counting task are presented in Table 71. This table reports the performance of each model or baseline method based on Precision, Recall, F1-Score, and Root Mean Square Error (RMSE) metrics.

### 7.2. BEV Lane Designation Recognition

In the lane designation recognition task, we introduce a rule-driven mapping table based on traffic common sense as a baseline:

- **1 lane:** The single lane is assigned as `left-turn`, `straight`, or `right-turn`.
- **2 lanes:** The first lane (leftmost) is designated as `left-turn` or `straight`, and the second lane (rightmost) as `straight` or `right-turn`.
- **3 or more lanes:** The first lane (leftmost) is designated as `left-turn`, the last lane (rightmost) as `right-turn`, and all intermediate lanes as `straight`.

Table 72 provides the complete results for the BEV lane designation recognition task. The models and baseline methods are evaluated using Hamming Loss and Accuracy.

### 7.3. BEV Road Network Correction

The comprehensive results for the BEV road network correction task are shown in Table 73. This task evaluates model performance on junctions by RMSE and road segments by Fréchet Distance (FD) at different normalized distance upper bound thresholds.

### 7.4. FPV Lane Counting

The results for the FPV lane counting task are summarized in Table 74. The table includes Precision, Recall, F1-Score, and RMSE for each model and baseline method.

Table 71. The complete experimental results of the BEV lane counting task. The best-performing result among the evaluated models is indicated in **bold**, and the second-best result is indicated with an underline.

| Model                  | Precision $\uparrow$ | Recall $\uparrow$ | F1-Score $\uparrow$ | RMSE $\downarrow$ |
|------------------------|----------------------|-------------------|---------------------|-------------------|
| LLaMA-3.2-11B-Vision   | 0.2707               | 0.2586            | 0.2415              | 1.5792            |
| LLaMA-3.2-90B-Vision   | 0.2904               | 0.3109            | 0.2947              | 1.3344            |
| Qwen2.5-VL-7B          | 0.2718               | 0.2871            | 0.2412              | 1.4091            |
| Qwen2.5-VL-32B         | 0.2882               | 0.3181            | 0.2804              | 1.2430            |
| Qwen2.5-VL-72B         | 0.2994               | 0.2830            | 0.2053              | 1.3420            |
| Gemma-3-12B            | 0.2529               | 0.3349            | 0.2223              | 1.1937            |
| Gemma-3-27B            | 0.2817               | 0.3188            | 0.2785              | 1.3314            |
| Gemini-2.5-Flash       | 0.2816               | 0.2847            | 0.2387              | 1.4192            |
| Gemini-2.5-Flash-Image | 0.2718               | 0.2892            | 0.2360              | 1.3721            |
| Gemini-2.5-Pro         | 0.3286               | 0.3415            | <u>0.3218</u>       | 1.2495            |
| GLM-4.5V               | 0.3084               | <u>0.3528</u>     | 0.3155              | 1.1765            |
| GPT-5-Nano             | 0.2530               | 0.2596            | 0.1884              | 1.5107            |
| GPT-5-Mini             | <b>0.3863</b>        | <b>0.3931</b>     | <b>0.3693</b>       | <u>1.1515</u>     |
| GPT-5                  | <u>0.3365</u>        | 0.3085            | 0.3095              | 1.3514            |
| Random Choice          | 0.2498               | 0.2882            | 0.2671              | <b>1.1093</b>     |
| Always 2-Lane          | 0.0637               | 0.2524            | 0.1017              | 1.5323            |

Table 72. The complete experimental results of the BEV lane designation recognition task. The best-performing result among the evaluated models is indicated in **bold**, and the second-best result is indicated with an underline.

| Model                  | Hamming Loss $\downarrow$ | Acc. $\uparrow$ |
|------------------------|---------------------------|-----------------|
| LLaMA-3.2-11B-Vision   | 0.3541                    | 0.1380          |
| LLaMA-3.2-90B-Vision   | 0.2075                    | 0.4705          |
| Qwen2.5-VL-7B          | 0.2965                    | 0.1031          |
| Qwen2.5-VL-32B         | 0.2258                    | 0.3839          |
| Qwen2.5-VL-72B         | 0.2044                    | 0.4775          |
| Gemma-3-12B            | 0.2496                    | 0.3493          |
| Gemma-3-27B            | 0.2053                    | 0.4146          |
| Gemini-2.5-Flash       | 0.1955                    | 0.4830          |
| Gemini-2.5-Flash-Image | 0.1807                    | 0.4938          |
| Gemini-2.5-Pro         | 0.1640                    | 0.5375          |
| GLM-4.5V               | 0.1679                    | 0.5461          |
| GPT-5-Nano             | 0.1638                    | 0.5541          |
| GPT-5-Mini             | <u>0.1516</u>             | 0.5557          |
| GPT-5                  | <u>0.1557</u>             | <u>0.5855</u>   |
| Rule-based             | <b>0.1413</b>             | <b>0.6047</b>   |

## 7.5. FPV Lane Designation Recognition

Table 75 displays the complete experimental outcomes for the FPV lane designation recognition task, measured by Hamming Loss and Accuracy.

## 7.6. FPV Road Type Classification

The performance of all models on the FPV road type classification task is detailed in Table 76, with results reported in Accuracy.

## 8. Results of Further Analysis

### 8.1. The Impact of Reference Line Prompting Methods in the BEV Tasks

The experimental results of the impact of reference line prompting methods in the BEV tasks are shown in Table 87 and Table 88. For all results, the relative change ratios of metrics for other prompting methods were calculated relative to the benchmark default settings (both prompts with arrows)

Table 73. The complete experimental results of the BEV road network correction task. The best-performing result among the evaluated models is indicated in **bold**, and the second-best result is indicated with an underline.

| Model                  | Junction      |               |               | Road Segment  |               |               |
|------------------------|---------------|---------------|---------------|---------------|---------------|---------------|
|                        | RMSE@10% ↓    | RMSE@20% ↓    | RMSE@50% ↓    | FD@10% ↓      | FD@20% ↓      | FD@50% ↓      |
| LLaMA-3.2-11B-Vision   | 0.0934        | 0.1707        | 0.3323        | 0.0982        | 0.1891        | 0.3792        |
| LLaMA-3.2-90B-Vision   | 0.0843        | 0.1495        | 0.2720        | 0.0958        | 0.1745        | 0.3074        |
| Qwen2.5-VL-7B          | 0.0923        | 0.1699        | 0.3459        | 0.0981        | 0.1881        | 0.3976        |
| Qwen2.5-VL-32B         | 0.0872        | 0.1544        | 0.3185        | 0.0955        | 0.1709        | 0.3134        |
| Qwen2.5-VL-72B         | <u>0.0813</u> | <u>0.1375</u> | 0.2622        | 0.0918        | 0.1570        | 0.2586        |
| Gemma-3-12B            | 0.0875        | 0.1588        | 0.3179        | 0.0949        | 0.1717        | 0.2979        |
| Gemma-3-27B            | 0.0852        | 0.1432        | 0.2730        | 0.0934        | 0.1537        | <b>0.2320</b> |
| Gemini-2.5-Flash       | 0.0842        | 0.1482        | 0.3195        | 0.0958        | 0.1716        | 0.2808        |
| Gemini-2.5-Flash-Image | 0.0841        | 0.1462        | 0.3051        | 0.0963        | 0.1700        | 0.2700        |
| Gemini-2.5-Pro         | 0.0843        | 0.1444        | 0.3065        | 0.0964        | 0.1742        | 0.2934        |
| GLM-4.5V               | 0.0917        | 0.1706        | 0.3939        | <b>0.0899</b> | <u>0.1537</u> | 0.2711        |
| GPT-5-Nano             | <b>0.0798</b> | <b>0.1319</b> | <u>0.2603</u> | 0.0914        | <u>0.1537</u> | 0.2575        |
| GPT-5-Mini             | 0.0821        | 0.1391        | 0.2900        | <u>0.0907</u> | <b>0.1483</b> | <u>0.2409</u> |
| GPT-5                  | 0.0859        | 0.1418        | 0.2813        | 0.0951        | 0.1631        | 0.2608        |
| Do Nothing             | 0.0843        | 0.1554        | <b>0.2593</b> | 0.0997        | 0.1958        | 0.3807        |

Table 74. The complete experimental results of the FPV lane counting task. The best-performing result among the evaluated models is indicated in **bold**, and the second-best result is indicated with an underline.

| Model                  | Precision ↑   | Recall ↑      | F1-Score ↑    | RMSE ↓        |
|------------------------|---------------|---------------|---------------|---------------|
| LLaMA-3.2-11B-Vision   | 0.2717        | 0.2944        | 0.0000        | 1.4314        |
| LLaMA-3.2-90B-Vision   | 0.4003        | 0.3636        | 0.0000        | 1.1383        |
| Qwen2.5-VL-7B          | 0.3350        | 0.2822        | 0.2207        | 1.4161        |
| Qwen2.5-VL-32B         | 0.3978        | 0.3935        | 0.3354        | 1.0884        |
| Qwen2.5-VL-72B         | 0.4720        | 0.3826        | 0.3165        | 1.2010        |
| Gemma-3-12B            | 0.3694        | 0.2931        | 0.2199        | 1.2055        |
| Gemma-3-27B            | 0.3345        | 0.3134        | 0.2711        | 1.2060        |
| Gemini-2.5-Flash       | 0.4318        | 0.3758        | 0.3392        | 1.1759        |
| Gemini-2.5-Flash-Image | 0.4220        | 0.3569        | 0.2989        | 1.0000        |
| Gemini-2.5-Pro         | <u>0.5399</u> | <u>0.5183</u> | <u>0.5093</u> | <u>0.8940</u> |
| GLM-4.5V               | 0.4746        | 0.4179        | 0.3817        | 0.9973        |
| GPT-5-Nano             | 0.4236        | 0.3677        | 0.2890        | 1.2519        |
| GPT-5-Mini             | 0.4909        | 0.4532        | 0.4117        | 0.9311        |
| GPT-5                  | <b>0.5652</b> | <b>0.5455</b> | <b>0.5261</b> | <b>0.8367</b> |
| Random Choice          | 0.2065        | 0.2497        | 0.2245        | 1.4404        |
| Always 2-Lane          | 0.0644        | 0.2537        | 0.1027        | 1.6111        |

to visualize the differences.

## 8.2. The Impact of Scene Environment Conditions in the FPV Tasks

The experimental results of the impact of scene environment conditions in the FPV tasks are shown in Table 89, Table 810, and Table 811. For all results, the relative change ratios of metrics for other prompting methods were calculated relative to those of the full datasets to visualize the differences.

## 9. Case Analysis

This section presents a detailed analysis of failure cases across different tasks in RoadBench, highlighting common failure patterns and limitations of current MLLMs in fine-grained spatial understanding and reasoning under urban road scenarios. In the following analyzes, we selected the evaluation results of the MLLMs that ranked highly in the benchmarks corresponding to the tasks to be analyzed. In the

Table 75. The complete experimental results of the FPV lane designation recognition task. The best-performing result among the evaluated models is indicated in **bold**, and the second-best result is indicated with an underline.

| Model                  | Hamming Loss ↓ | Acc. ↑        |
|------------------------|----------------|---------------|
| LLaMA-3.2-11B-Vision   | 0.3492         | 0.1586        |
| LLaMA-3.2-90B-Vision   | 0.1609         | 0.5246        |
| Qwen2.5-VL-7B          | 0.2869         | 0.1669        |
| Qwen2.5-VL-32B         | 0.2316         | 0.3233        |
| Qwen2.5-VL-72B         | 0.1809         | 0.4807        |
| Gemma-3-12B            | 0.2369         | 0.3642        |
| Gemma-3-27B            | 0.2019         | 0.4037        |
| Gemini-2.5-Flash       | 0.1703         | 0.5085        |
| Gemini-2.5-Flash-Image | 0.1773         | 0.4794        |
| Gemini-2.5-Pro         | 0.1429         | 0.5693        |
| GLM-4.5V               | 0.1430         | 0.5793        |
| GPT-5-Nano             | 0.1500         | 0.5441        |
| GPT-5-Mini             | 0.1301         | <u>0.5941</u> |
| GPT-5                  | <u>0.1287</u>  | 0.5932        |
| Rule-based             | <b>0.1282</b>  | <b>0.6019</b> |

Table 76. The complete experimental results of the FPV road type classification task. The best-performing result among the evaluated models is indicated in **bold**, and the second-best result is indicated with an underline.

| Model                  | Acc. ↑        |
|------------------------|---------------|
| LLaMA-3.2-11B-Vision   | 0.5530        |
| LLaMA-3.2-90B-Vision   | 0.6398        |
| Qwen2.5-VL-7B          | 0.5298        |
| Qwen2.5-VL-32B         | 0.5631        |
| Qwen2.5-VL-72B         | 0.5954        |
| Gemma-3-12B            | 0.5752        |
| Gemma-3-27B            | 0.5237        |
| Gemini-2.5-Flash       | 0.5560        |
| Gemini-2.5-Flash-Image | 0.5691        |
| Gemini-2.5-Pro         | <b>0.7639</b> |
| GLM-4.5V               | 0.5984        |
| GPT-5-Nano             | 0.6115        |
| GPT-5-Mini             | 0.6065        |
| GPT-5                  | <u>0.7053</u> |
| Random Choice          | 0.5045        |

text description of each failure case, the text in the **Analysis** paragraph is a brief error description provided after manual checking, not a model output.

### 9.1. BEV Lane Counting

This subsection presents failure cases generated by GPT-5-Mini in BEV lane counting tasks.

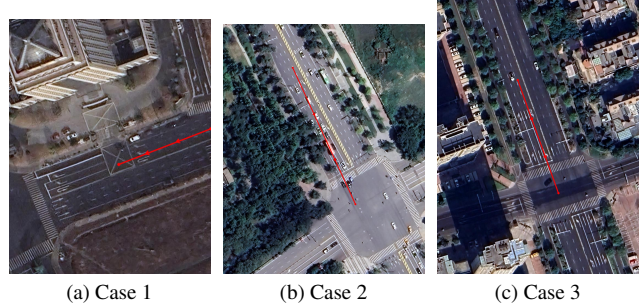


Figure 97. Example images of BEV lane counting failure cases.

#### Case 1:

##### MLLM Response:

```
```yaml
# Explanation: I counted the distinct
  through-lane markings and dashed
  separators in the marked
  carriageway - there are four
  parallel through lanes for traffic
  moving in the arrow direction
num_lanes: 4
```
```

##### Ground Truth:

```
```yaml
num_lanes: 3
```
```

**Analysis:** The model failed to infer that the rightmost lane is a non-motorized vehicle lane based on the presence of ground markings, leading to an overcount of lanes.

#### Case 2:

##### MLLM Response:

```
```yaml
# Explanation: The marked carriageway
  (right-side traffic flow) shows
  three distinct lane markings/queues
  (three rows of vehicles and two
  dashed separators) indicating three
  lanes in the arrow direction
num_lanes: 3
```
```

##### Ground Truth:

```
```yaml
num_lanes: 4
```
```

**Analysis:** The model failed to reason that the left-most lane, despite having no vehicles, is still a motor vehicle lane, resulting in an undercount.

Table 87. GLM-4.5V performance comparison with different prompt strategies. The best-performing result among the evaluated models is indicated in **bold**, and the second-best result is indicated with an underline.

| Method              | BEV Lane Counting      |                        | BEV Lane Designation Recognition |                        |
|---------------------|------------------------|------------------------|----------------------------------|------------------------|
|                     | F1-Score $\uparrow$    | RMSE $\downarrow$      | Hamming Loss $\downarrow$        | Acc. $\uparrow$        |
| Text-only           | 0.3116 (-1.24%)        | 1.3535 (+15.04%)       | 0.1847 (+10.01%)                 | 0.4924 (-9.83%)        |
| Visual-only (Color) | <b>0.3184 (+0.92%)</b> | 1.1904 (+1.18%)        | 0.1701 (+1.31%)                  | 0.5389 (-1.32%)        |
| Visual-only (Arrow) | 0.3088 (-2.12%)        | <b>1.1496 (-2.29%)</b> | <u>0.1694 (+0.89%)</u>           | 0.5426 (-0.64%)        |
| Both (Color)        | 0.3131 (-0.76%)        | 1.2820 (+8.97%)        | 0.1697 (+1.07%)                  | <u>0.5439 (-0.40%)</u> |
| Both (Arrow)        | <u>0.3155 (-)</u>      | <u>1.1765 (-)</u>      | <b>0.1679 (-)</b>                | <b>0.5461 (-)</b>      |

Table 88. GPT-5-Mini performance comparison with different prompt strategies. The best-performing result among the evaluated models is indicated in **bold**, and the second-best result is indicated with an underline.

| Method              | BEV Lane Counting      |                        | BEV Lane Designation Recognition |                        |
|---------------------|------------------------|------------------------|----------------------------------|------------------------|
|                     | F1-Score $\uparrow$    | RMSE $\downarrow$      | Hamming Loss $\downarrow$        | Acc. $\uparrow$        |
| Text-only           | 0.3379 (-8.50%)        | 1.2419 (+7.85%)        | 0.1491 (-1.65%)                  | 0.5613 (+1.01%)        |
| Visual-only (Color) | <u>0.3606 (-2.36%)</u> | 1.1867 (+3.06%)        | <u>0.1467 (-3.23%)</u>           | 0.5657 (+1.80%)        |
| Visual-only (Arrow) | 0.3500 (-5.23%)        | 1.1671 (+1.35%)        | 0.1478 (-2.51%)                  | <u>0.5679 (+2.20%)</u> |
| Both (Color)        | 0.3569 (-3.36%)        | <b>1.1428 (-0.76%)</b> | <b>0.1465 (-3.36%)</b>           | <b>0.5682 (+2.25%)</b> |
| Both (Arrow)        | <b>0.3693 (-)</b>      | <u>1.1515 (-)</u>      | 0.1516 (-)                       | 0.5557 (-)             |

**Case 3:**

**MLLM Response:**

```
```yaml
# Explanation: I inspected the
  carriageway on the side
  corresponding to the arrow (right-
  hand driving). I can see four
  distinct parallel traffic lanes
  heading in the arrow direction (
  multiple through lanes plus a
  rightmost turn/through lane) based
  on the painted lane markings and
  turn bays.
```

```
num_lanes: 4
```
```

**Ground Truth:**

```
```yaml
num_lanes: 3
```
```

**Analysis:** The model demonstrates poor understanding of bidirectional roads, incorrectly counting lanes from the opposite direction’s arrow markings as part of the current direction’s lane count.

**Summary:** In this task, MLLMs show their shortcomings in understanding and reasoning about the identification of fine-grained spatial elements and the associations between elements. Case 3 exemplifies the failure of MLLMs to recognize arrows in the opposite direction. Case 1 and Case 2, on the other hand, show that MLLMs are unable to effectively

integrate the complex relationship between vehicles and road markings.

**9.2. BEV Lane Designation Recognition**

This subsection presents failure cases generated by GPT-5 in BEV lane designation recognition tasks.



(a) Case 1

(b) Case 2

Figure 98. Example images of BEV lane designation failure cases.

**Case 1:**

**MLLM Response:**

```
```yaml
# Explanation: Near the intersection,
  lane arrows are visible-leftmost
  shows a left-turn, the next shows
  both left-turn and straight, the
  middle two show straight-only
  arrows, and the far-right lane
```

Table 89. GLM-4.5V performance analysis across different environmental conditions.

Condition	FPV Lane Counting		FPV Lane Designation Recognition	
	F1-Score ↑	RMSE ↓	Hamming Loss ↓	Accuracy ↑
Adverse Lighting Conditions	0.3283 (-14.0%)	1.0170 (+2.0%)	0.1509 (+5.5%)	0.5434 (-6.2%)
Obscured Road Markings	0.3838 (+0.6%)	1.0632 (+6.6%)	0.1271 (-11.1%)	0.5543 (-4.3%)
All	0.3817 (-)	0.9973 (-)	0.1430 (-)	0.5793 (-)

Table 810. GPT-5 performance analysis across different environmental conditions.

Condition	FPV Lane Counting		FPV Lane Designation Recognition	
	F1-Score ↑	RMSE ↓	Hamming Loss ↓	Accuracy ↑
Adverse Lighting Conditions	0.5272 (+0.2%)	0.8485 (+1.4%)	0.1311 (+1.9%)	0.5887 (-0.8%)
Obscured Road Markings	0.4674 (-11.2%)	0.9555 (+14.2%)	0.1371 (+6.5%)	0.5543 (-6.6%)
All	0.5261 (-)	0.8367 (-)	0.1287 (-)	0.5932 (-)

```

shows a right-turn arrow.
lane_designations: [{"left-turn"}, [{"
left-turn", "straight"}, [{"straight
"}, [{"straight"}, [{"right-turn"}]
...

```

Ground Truth:

```

```yaml
lane_designations: [{"U-turn", "left-
turn"}, [{"straight"}, [{"straight"},
["straight"}, [{"right-turn"}]
...

```

**Analysis:** The model failed to identify a U-turn lane that is located before the junction, demonstrating insufficient understanding of transportation system markings and road design patterns.

```

...

```

**Analysis:** The model failed to understand that this is a bidirectional road and incorrectly searched for left-turn lanes in the lower portion of the image instead of recognizing the left-turn lane in the current direction.

**Summary:** In this task, MLLMs similarly demonstrate a lack of fine-grained road marking recognition (Case 1) and a lack of understanding of the road marking system (Case 2).

**9.3. BEV Road Network Correction**

This subsection presents failure cases generated by Gemma-3-27B in BEV road network correction tasks. In the images for this task, the red lines represent the inputs to the MLLMs, the blue lines represent the outputs of the MLLMs, and the green lines represent the truth values labeled in the dataset.

**Case 2:**

**MLLM Response:**

```

```yaml
# Explanation: On the east approach (
right side) the three lanes next to
a separate channelized right-turn
slip lane show straight arrows,
with left-turn lanes segregated by
islands-so the through carriageway
is straight-only.
lane_designations: [{"straight"}, [{"
straight"}, [{"straight"}]
...

```

Ground Truth:

```

```yaml
lane_designations: [{"left-turn"}, [{"
straight"}, [{"straight"}]

```

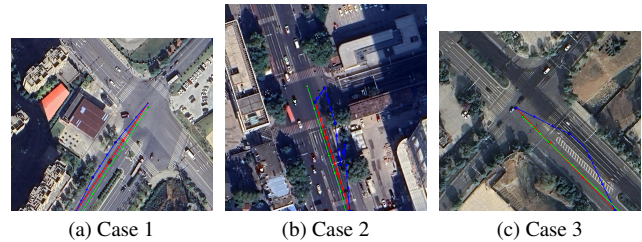


Figure 99. Example images of BEV road network correction failure cases.

**Case 1:**

**MLLM Response:**

```

```yaml

```

Table 811. Gemini-2.5-Pro performance analysis across different environmental conditions.

Condition	FPV Lane Counting		FPV Lane Designation Recognition	
	F1-Score ↑	RMSE ↓	Hamming Loss ↓	Accuracy ↑
Adverse Lighting Conditions	0.4932 (-3.2%)	0.9442 (+5.6%)	0.1462 (+2.3%)	0.5491 (-3.5%)
Obscured Road Markings	0.6369 (+25.1%)	0.7518 (-15.9%)	0.1357 (-5.0%)	0.5257 (-7.7%)
All	0.5093 (-)	0.8940 (-)	0.1429 (-)	0.5693 (-)

```
# Explanation: Identified two
junctions where the road splits/
intersects and created line
segments connecting them based on
the reference line's direction.
Corrected the line segments to
follow the actual road centerlines.
junctions: ["POINT (641 640)", "POINT
(501 855)"]
lines: ["LINESTRING (840 400, 641 640)
", "LINESTRING (641 640, 501 855)",
"LINESTRING (501 855, 400 1062)"]
```
```

**Analysis:** The model cannot precisely determine the location of junctions, leading to inaccurate junction coordinates and incorrect road network topology.

**Case 2:  
MLLM Response:**

```
```yaml
# Explanation: Added junctions at the
intersection identified in the
image and split the original line
into multiple segments following
the road centerline. Corrected the
path to accurately reflect traffic
flow.
junctions: ["POINT (536 581)", "POINT
(484 409)", "POINT (437 478)", "
POINT (607 1009)", "POINT (558 783)
", "POINT (580 685)"]
lines: ["LINESTRING (607 1009, 580
685)", "LINESTRING (580 685, 558
783)", "LINESTRING (558 783, 536
581)", "LINESTRING (536 581, 484
409)", "LINESTRING (484 409, 437
478)"]
```
```

**Analysis:** The model cannot output stable coordinates, producing inconsistent and unreliable junction and line segment positions across different reasoning attempts.

**Case 3:  
MLLM Response:**

```
```yaml
# Explanation: The reference line
missed the intersection. I added a
junction at the intersection and
split the line into two segments
accordingly.
junctions: ["POINT (400 400)", "POINT
(681 534)", "POINT (919 937)"]
lines: ["LINESTRING (400 400, 515 454,
602 500, 681 534)", "LINESTRING
(681 534, 761 604, 863 818, 919
937)"]
```
```

**Analysis:** While the model recognizes that a junction is missing, it cannot accurately determine the direction of bidirectional roads, leading to incorrect road network topology.

**Summary:** Road network correction failures expose significant challenges in spatial reasoning: (1) imprecise junction localization, where models struggle to accurately identify intersection locations, (2) coordinate instability, resulting in inconsistent outputs across different reasoning attempts, and (3) difficulty in understanding bidirectional road configurations, leading to incorrect direction assignments in the road network.

**9.4. FPV Lane Counting**

This subsection presents failure cases generated by GPT-5 in FPV lane counting tasks.



(a) Case 1



(b) Case 2

Figure 910. Example images of FPV lane counting failure cases.

**Case 1:****MLLM Response:**

```
```yaml
# Explanation: The wet road shows
  three parallel lanes with visible
  lane dividers and arrow markings,
  indicating three lanes moving in
  our direction.
num_lanes: 3
```
```

**Ground Truth:**

```
```yaml
num_lanes: 5
```
```

**Analysis:** Under poor nighttime lighting conditions, the model cannot utilize overhead arrow signs to infer the number of lanes, relying solely on visible ground markings which are insufficient in low-light scenarios.

**Case 2:****MLLM Response:**

```
```yaml
# Explanation: Three distinct lanes
  are visible on our side-left next
  to the double yellow centerline, a
  middle lane, and a rightmost lane
  by the curb-separated by dashed
  white lines and lane arrows.
num_lanes: 3
```
```

**Ground Truth:**

```
```yaml
num_lanes: 5
```
```

**Analysis:** The model cannot understand that opposite-direction lanes are unrelated to the current direction and should not be included in the lane count calculation.

**Summary:** In the FPV perspective, MLLMs are further exposed for their problems in urban roadway marking and spatial understanding, especially for misrecognition and understanding of opposing lanes. In addition, poor lighting conditions are one of the challenges for the application of MLLMs in realistic urban scenarios.

## 9.5. FPV Lane Designation Recognition

This subsection presents failure cases generated by GPT-5 in FPV lane designation recognition tasks.



(a) Case 1



(b) Case 2

Figure 911. Example images of FPV lane designation failure cases.

**Case 1:****MLLM Response:**

```
```yaml
# Explanation: The center lane clearly
  shows a straight arrow marking,
  and typical Chinese intersection
  layout plus the overhead lane sign
  suggest the left lane is for left-
  turns and the right lane is for
  right-turns.
lane_designations: [{"left-turn"}, {"
  straight"}, {"right-turn"}]
```
```

**Ground Truth:**

```
```yaml
lane_designations: [{"straight"}, {"
  straight"}, {"straight"}]
```
```

**Analysis:** The model relies excessively on common sense reasoning rather than visual information from the image, leading to incorrect lane function assignments based on typical intersection layouts rather than actual road markings.

**Case 2:****MLLM Response:**

```
```yaml
# Center lane clearly shows a straight
  arrow; rightmost lane marking
  shows straight and right-turn;
  leftmost lane has no visible turn
  markings, so assumed straight
lane_designations: [{"straight"}, {"
  straight"}, {"straight", "right-
  turn"}]
```
```

**Ground Truth:**

```
```yaml
lane_designations: [{"straight"}, {"
  straight"}, {"straight"}]
```
```

**Analysis:** The model incorrectly identifies lanes from

the opposite direction as lanes in the current direction, demonstrating confusion in bidirectional road scenarios.

**Summary:** Similarly, MLLMs are still not effective in this task to correctly understand lane direction and make correct inferences based on road markings as well as vehicle orientation. Also in nighttime environments, MLLMs seem to give up reasoning using road marking information that is recognizable to the human eye, and instead rely on common sense.

## 9.6. FPV Road Type Classification

This subsection presents failure cases generated by Gemini-2.5-Pro in FPV road type classification tasks.



Figure 912. Example images of FPV road type classification failure cases.

### Case 1:

#### MLLM Response:

```
```yaml
# Explanation: The vehicle is on a
  multi-lane road running parallel to
  another traffic system, separated
  by a yellow guardrail, which is a
  common design for a service road (
  auxiliary road) alongside a main
  road or expressway.
road_type: "service"
```
```

#### Ground Truth:

```
```yaml
road_type: "main"
```
```

**Analysis:** The model cannot correctly identify that the central guardrail serves to separate bidirectional lanes rather than separate a service road from a main road, leading to incorrect road type classification.

### Case 2:

#### MLLM Response:

```
```yaml
# Explanation: The image displays a
  wide, multi-lane road with an
  elevated highway to the left and a
  large overhead traffic sign in the
  distance, all indicative of a
  primary traffic artery rather than
  a smaller, auxiliary service road.
road_type: "main"
```
```

#### Ground Truth:

```
```yaml
road_type: "service"
```
```

**Analysis:** The model incorrectly associates overhead signs and elevated structures in the distance with the current road, failing to recognize that these elements belong to a different road system rather than the current roadway.

**Summary:** Similarly, MLLMs still struggle with understanding lane direction. Meanwhile, the behavior of randomly associating visual elements hints at the risk of applying MLLMs in reality.

By observing the failures of SOTA MLLMs under each task in RoadBench, we gain further insights into the inadequacy of existing MLLMs in terms of their ability to understand and reason about fine-grained spatial elements. On the one hand, MLLMs are not good at identifying and incorporating into reasoning high information content targets that are smaller, fuzzier, or closer to the surrounding color. On the other hand, MLLMs do not do a good job of integrating expert knowledge (e.g., how to distinguish between two-way lanes) with visual elements to enable reasoning about relationships between fine-grained spatial elements. These insights also further illustrate the research value of RoadBench.